CHAPTER IV
RESULTS AND DISCUSSION

4.1 Spirulina Strain Classification by FTIR and PLS-DA

Discovery of Spirulina morphology. In the study of strain classification, we observed the differentiate of helical and the length that similar like other Spirulina (Wang, Z. P., & Zhao, Y. 2005: Nowicka-Krawczyk, P., et al 2019: Sinetova, M. A., et al 2024). The Spirulina strains (H53, SB, SL, SBL, Rev, C005L, and C005H) were observed under light microscopy. Strain H53 presented an open helix cylindrical shape typical of Spirulina. Also, strain SB showed visibly thicker trichomes than strain H53, while strain SL had slightly longer filaments but a coil structure similar to that of H53 strain. The SBL strain consisted of SB traits with longer filaments. Similarly, strain Rev showed a reversed helical as opposed to the H53 stain. Distinctly, C005L consists of straight, non-helical filaments, unlike all other strains. Also, the C005H strain stood out with notably long trichomes.

The growth curves of all seven Spirulina strains (H53, R, SBL, SL, C005L, C005H, and SB) cultured in Zarrouk's medium at 25°C were observed with the identification of their stationary phases (Figure 4.1). The mid-log phase of each strain was reached at different time points. Strain H53 reached this phase earliest on day 7, followed by strains R, SB, SL, C005H, and C005L on day 8. Strain SBL exhibited the latest mid-log phase on day 9. These showed different growth patterns with optical density (OD_{560}). These results were aligned with previous studies on S. platensis cultivation (Shi et al., 2016; da Silva et al., 2016). These strains were appropriate representatives for FTIR analysis due to their biochemical composition during the stationary phase.

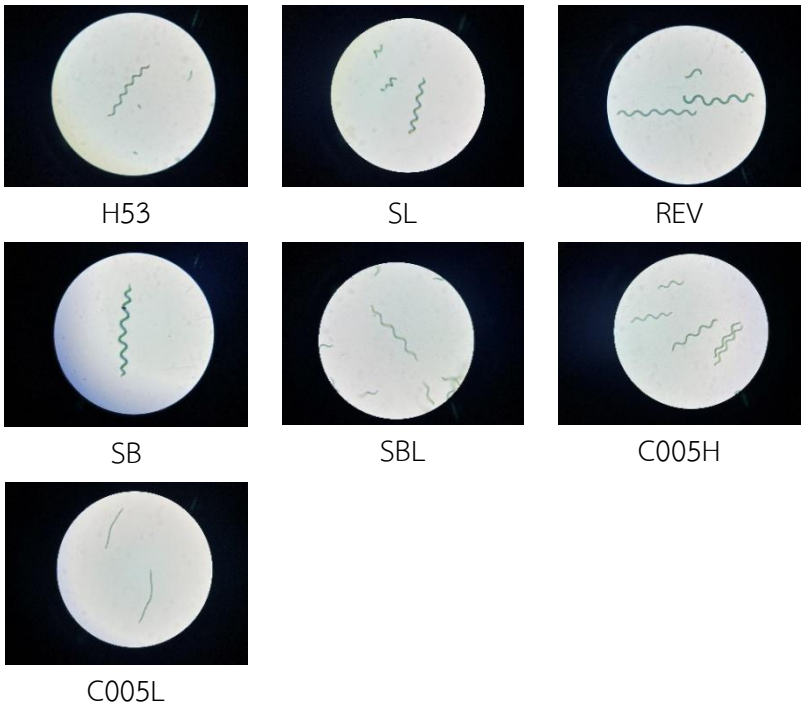

Figure 4.1 Morphological comparison of seven Spirulina strains (H53, SB, SL, SBL, Rev, C005L, C005H) under light microscopy

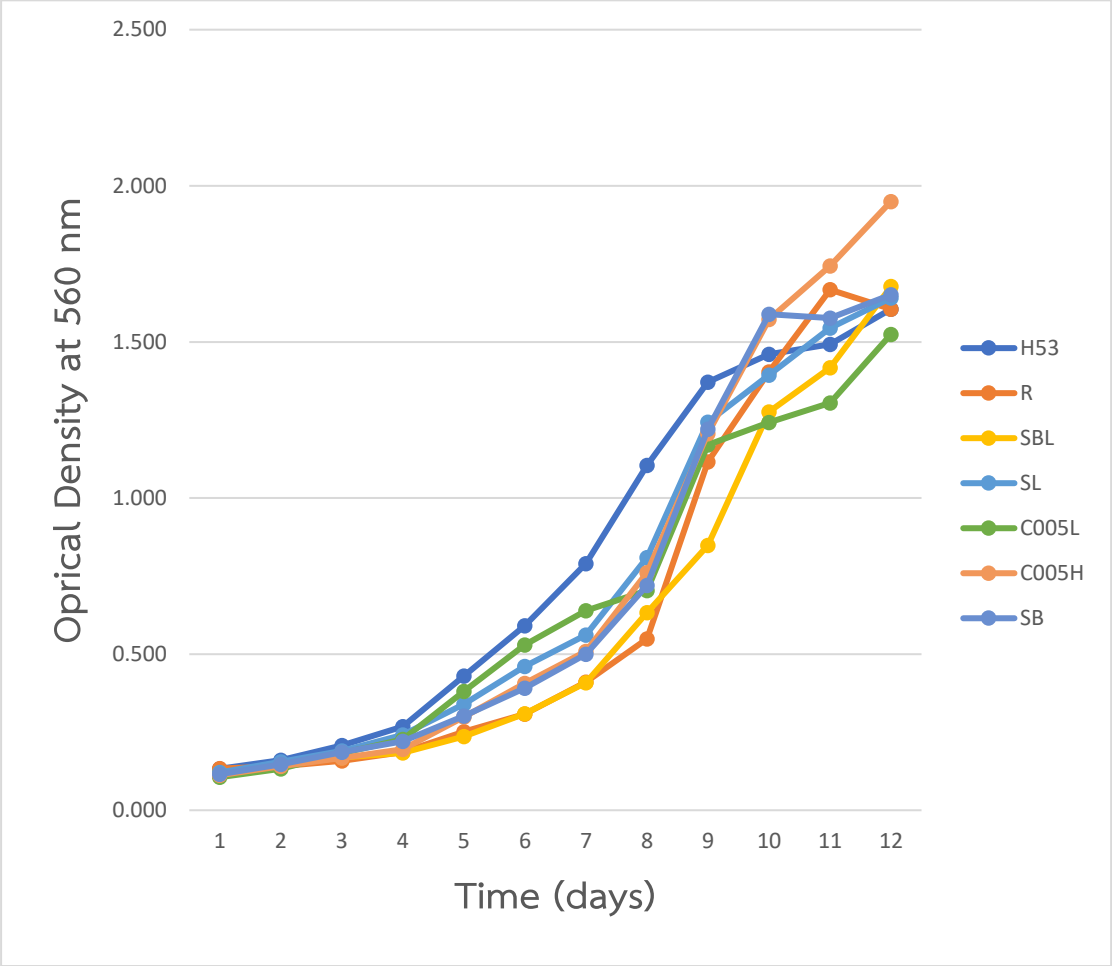

Figure 4.2 Growth curves of seven Spirulina strains measured by optical density at 560 nm (OD_{560}) over the cultivation period

Fourier transform infrared (FTIR) spectroscopy, it is a technique used to identify and classify microbes Since 1991 (Wenning et al., 2013). The mid-IR spectroscopy uses wave numbers between approximately 400 and 4000 cm^{-1}. The principle in the FTIR technique is a spectroscopy method used to identify variations in microorganisms total composition by detecting changes in functional groups in biomolecules including proteins, carbohydrates, lipids, and nucleic acids, absorb infrared light at particular wavelengths. Multivariate statistical analysis is used in the data evaluation process.

therefore, this method has rapid screening and potential approach for determine the correlation of biochemical profile in Spirulina. Because it is a technique that specific analyzed, time efficiency, minimal sample requirement, It is safe for humans and the environment and does not react with samples, making it an effective tool for rapid screening and precise high energy throughput characterization while safeguarding public health, the environment and product. (Wu, T. et al., 2018; Mazivila, et al., 2015) by this technique has been used in identification and characterization of some species of Cyanobacteria, Chlorophyta and Bacillariophyta (Özer, T., et al., 2016)

The study revealed that FTIR spectroscopy could determine biochemical profile of Spirulina among 7 strains such as H53, Reverse, SB (super blue), SBL (super blue long), SL (super long), C005H and C005L. The Strain was analyzed. Characteristic bands showed cellular components that were observed in all samples. Especially, the peak region at 3,100-2,800 cm-1 aligned with the vibrational of CH=CH in lipids region and carotenoids, the peak region at 1,700–1,500 cm^{-1} was characterized by amide bands in proteins and the peaks at the 1,200–900 cm^{-1} range were primarily linked to C–O–C stretching vibrations. That has been found in polysaccharides. The dendrogram depicts dissimilarity that exists among the 7 strains sample that difference between their functional group ratio. The results revealed that protein, lipid and carbohydrate are the characteristics peak that found differently ratio in each strain.

Recently, consumers' perspective is lost faith in food product safety and quality (Lobstein, T. 2019). Thus, this study holds considerable potential for Spirulina quality control methodologies through FTIR technique, offering an alternative approach to assess biochemical composition and distinguish among cultivation conditions. FTIR technique can support the improvement of analytical quality to provide products and consumer confidence in the future. Additionally, the FTIR technique has been used to classify species and examine biochemical profile. (Özer, TF., et al., 2016; Nalimova, et al., 2005).

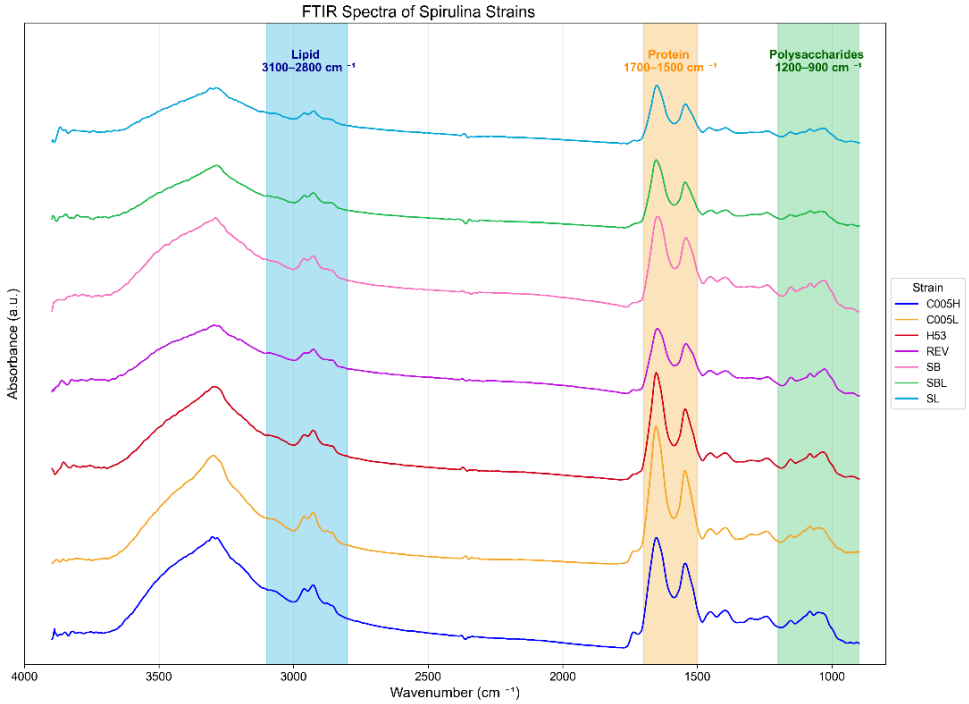

Figure 4.3 Average spectrum obtained from FTIR spectroscopy of 7 strains (H53, SB, SL, SBL, Rev, C005L, C005H)

In this study, the biochemical profile of Spirulina with independent variants, namely H53, Reverse, SB (Super Blue), SBL (Super Blue Long), SL (Super Long), C005H and C005L in controlled environment factors were studied. The biochemical profiles of the 7 species are shown in the figure (Figure 4.3). In the biomolecular level, it was found that the optimal three strains of Spirulina SB, C005L and C005H, which are align with previous research (Mróz et al 2024) that have successfully classified Spirulina. The peaks showing distinct differences among the three Spirulina strains appeared in the loading plot in the region of 1662–1513 cm^{-1} (proteins) and around 1020 cm^{-1} (polysaccharides), as presented in Figure 4.5.

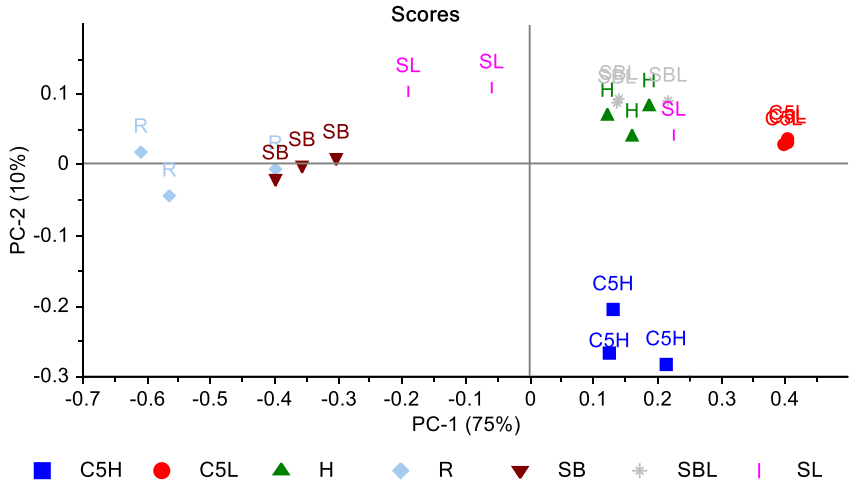

Figure 4.4 PCA score plot based on average FTIR spectra of 7 strains (H53, SB, SL, SBL, Rev, C005L, C005H)

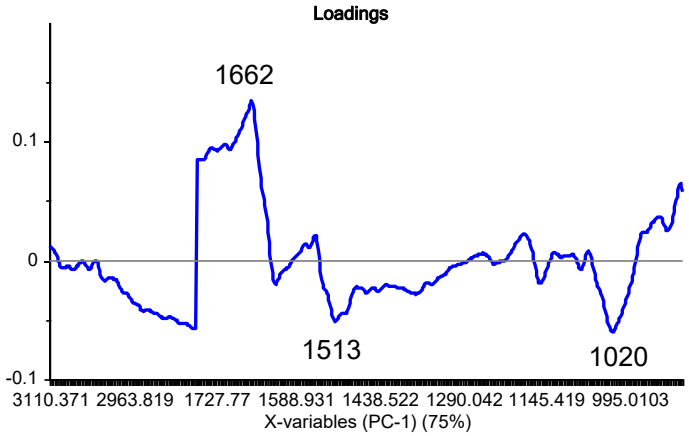

Figure 4.5 PCA loading plot (PC1) of FTIR spectra from C005H, C005L and SB strains

The model was created from the data of this experiment and consist of the coefficients of determination (R^2) were 0.945, 0.914, and 0.914 for SB, C005L, and

C005H-specific models, and the root mean squares error for the cross-validation (RMSECV) was 0.112, 0.140, and 0.140 for SB, C005L, and C005H models, respectively. This value is close to the value reported in the published research. (Wu, T., et al., 2018; Tarighat, M. A., et al 2022) The accuracy of models such as C005H achieved 81%, C005L achieved 93%, and SB achieved 97%. And these models had sensitivity value of 100%. Spectral data analysis from the FTIR technique was combined with PLS-DA data analysis in culture in the same control variable in this experiment (light, temperature, pH, it was suggested that FTIR in combination with PLS-DA was effective in classifying Spirulina strains.

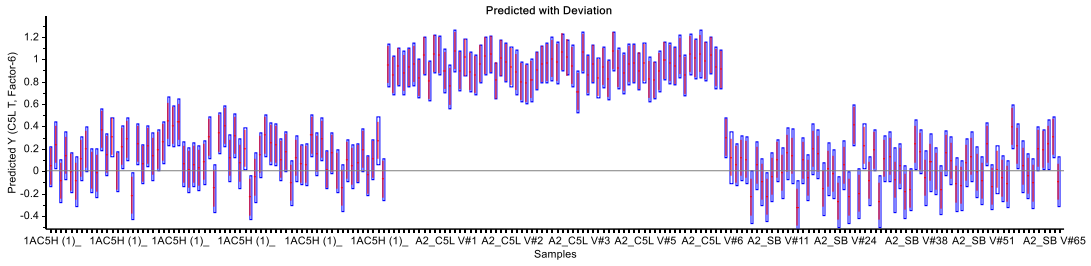

Figure 4.6 Distributions of reference and predicted values for the calibration sample sets from the C005H strains, C005L strains, and SB strains. Distributions of the reference and predicted values determined by the PLS-DA model

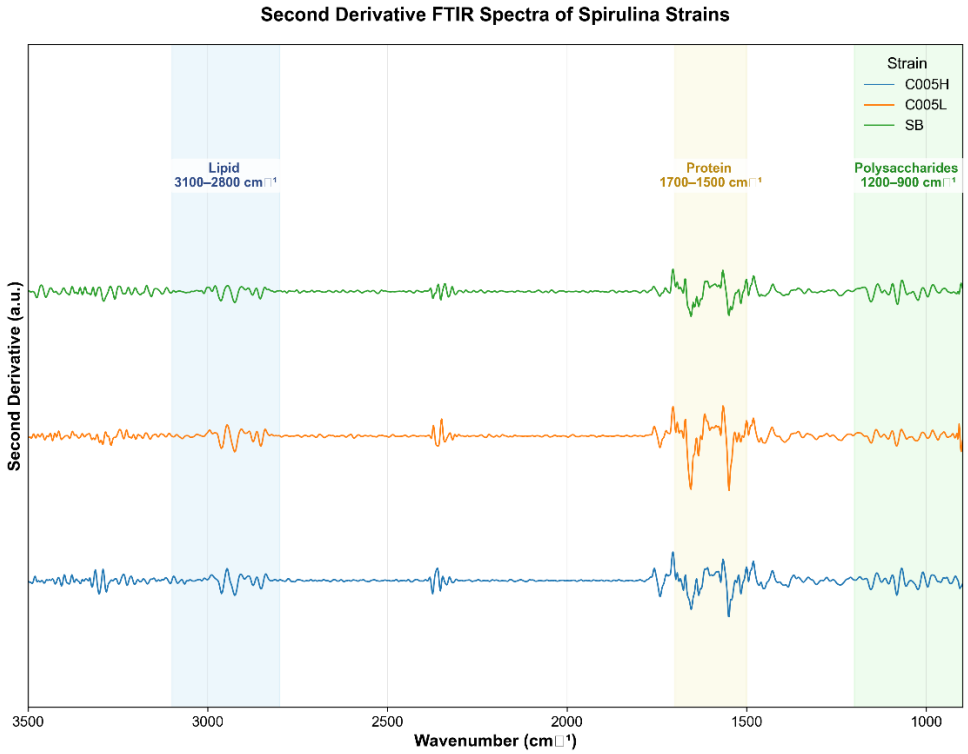

Figure 4.7 Second derivative of C005H, C005L and SB strains

The spectra in the lipid region showed similarity among the strains (Figure 4.8), which corresponds to the loading plot results.

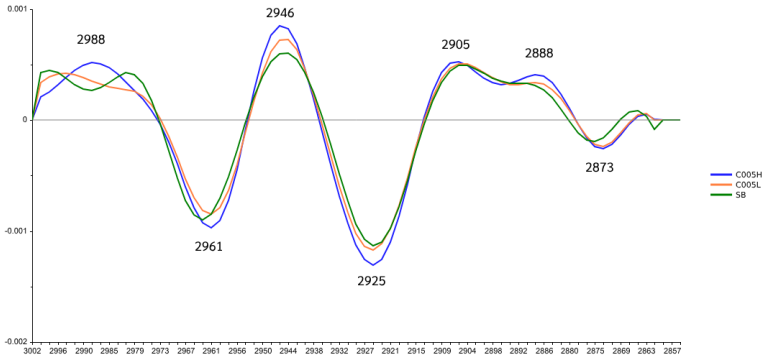

Figure 4.8 Second derivative FTIR spectra of C005H, C005L, and SB strains in the lipid region

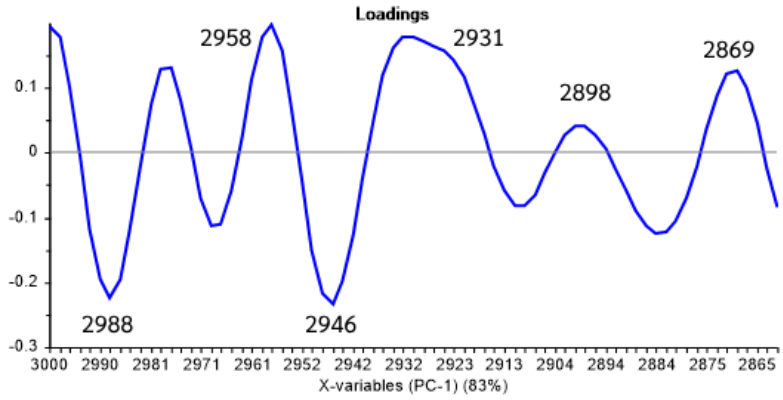

Figure 4.9 PCA loading plot (PC1) of FTIR spectra from of C005H, C005L, and SB strains in the lipid region

Based on the spectral data, the protein region showed the characteristic of peaks that among the strains. The main spectral difference was observed around 1656 cm^{-1}.

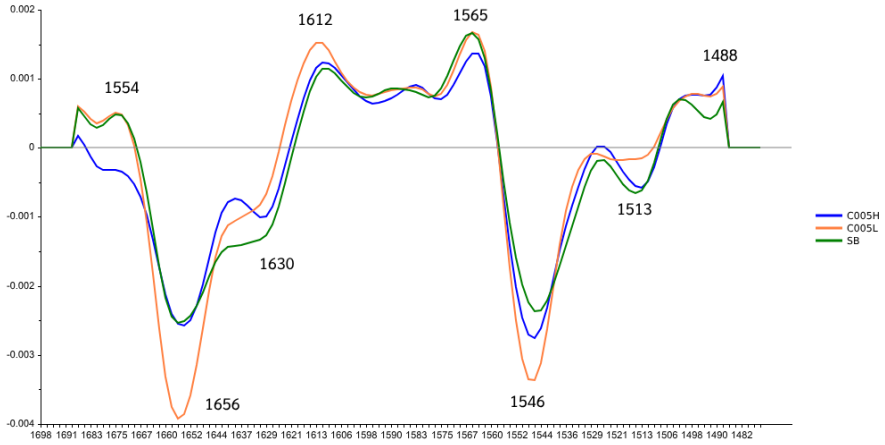

Figure 4.10 Second derivative FTIR spectra of C005H, C005L, and SB strains in the protein region

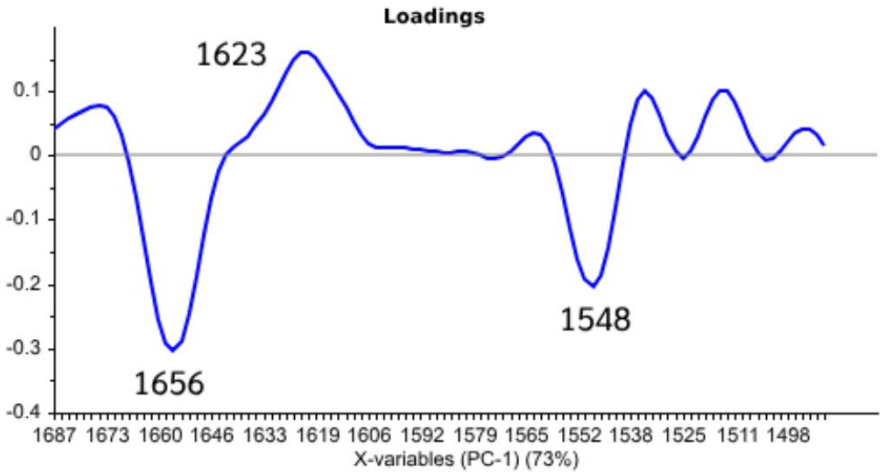

Figure 4.11 PCA loading plot (PC1) of FTIR spectra from of C005H, C005L, and SB strains in the protein region

In the polysaccharide region, several peaks showed noticeable differences among the strains, with the most distinct variation appearing around 1023 cm^{-1}.

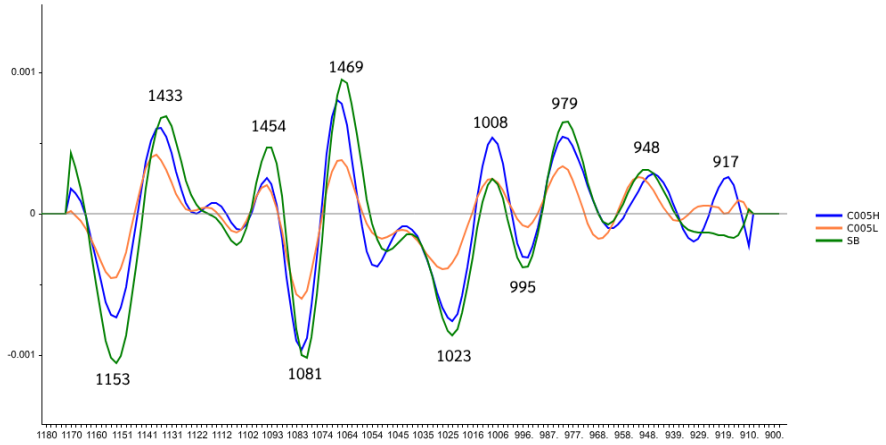

Figure 4.12 Second derivative FTIR spectra of C005H, C005L, and SB strains in the polysaccardes region

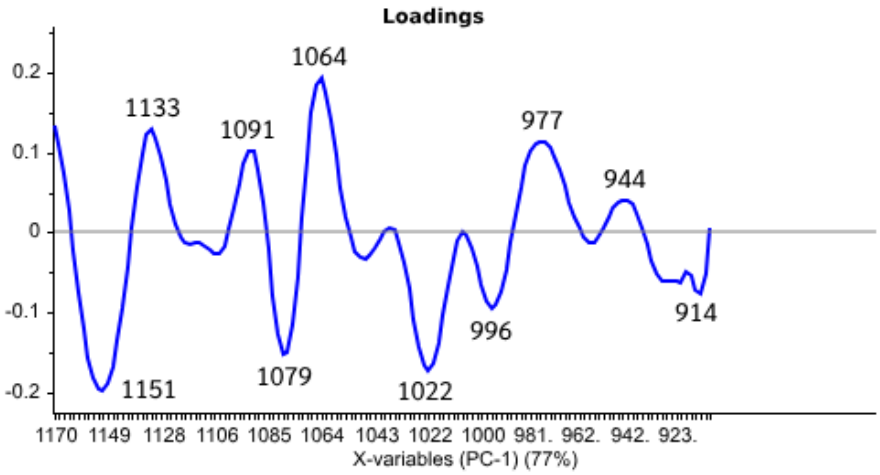

Figure 4.13 PCA loading plot (PC1) of FTIR spectra from of C005H, C005L, and SB strains in the polysaccardes region

The present tools for data analysis had lacked user-friendliness, Problem-specific software or scripts, or simply too hard to use. On the contrary, the Quasar evaluated supervised prediction methods, logistic regression and random experiment groups. The confusion matrix shows how well the SVM model can tell the difference between Spirulina strains. The numbers on the diagonal are the correctly identified samples, while the numbers off the diagonal show where the model got confused, meaning those strains have similar spectral patterns (Toplak, M., et al 2021).

The SVM focuses on the samples that are most similar to other strains, called support vectors. These points are used to create an optimal hyperplane or decision boundary, which helps the model decide the class of new observations in the future. This allows SVM to classify data efficiently and accurately.

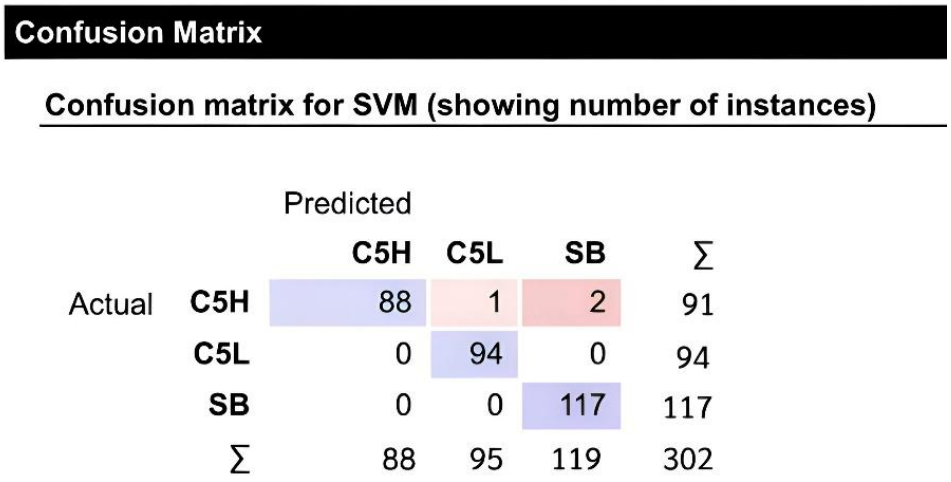

Figure 4.14 Confusion Matrix for Support Vector Machine (SVM) Classification of Astronomical Objects from Quasar Dataset

4.2 Effect of Light Conditions on Biochemical Profile of Spirulina H53

To investigate the biochemical profile effect of photoperiod length on the Spirulina H53, the strain was cultured under controlled indoor conditions using Zarrouk's medium, temperature (25°C) and pH 10, and three different light exposure durations (8, 12, and 24 hours). The FTIR spectra collected in the range of 4000–400 cm^{-1}. The treatment originally showed similar spectra signals among the treatments (Figure 4.15). The spectra determined peak regions corresponding to lipids, proteins, and polysaccharides. However, the spectra did not show visually distinguishable differences in the raw spectra.

There were noticeable differences after applying the second derivative transformation (Figure 4.16), especially in the protein region between 1700 and 1500 cm^{-1}. There was a noticeable difference at 1658 cm^{-1}, which corresponds to the amide I band of proteins but all three spectra showed consistent peak positions but differing intensities. This indicates that the length of the photoperiod influences the amount of protein compounds without changing their structure.

Further analysis showed loading line plots (Figure 4.22) revealed a considerable spectral region. These were found to be around 1685 to 1741 cm^{-1}. Protein signals are represented by this zone, which includes the amide I band, confirming that the main factor separating the light treatments was protein part.

The biochemical trends were visualized using cluster bar plots (Figure 4.18), which clearly show that protein signal quantity increased progressively with longer light exposure. This data corresponds with the numerical data in Table 4, where the protein content increased from 14.259 for 8 hours to 15.350 for 12 hours and 15.848 for 24 hours. This trend suggests a direct correlation between light exposure duration and protein synthesis.

Although lipid and polysaccharide signals showed some variation, they did not follow the same consistent trend as protein signal. While polysaccharide values rose at 12 hours (3.414) and slightly decreased at 24 hours (3.160), lipid values peaked at

12 hours (2.666) and then declined at 24 hours (2.184). Additionally, the 3D PCA model (Figure 4.19) supports the above findings by clearly separating the experimental groups based on their spectral profiles. The 8 hours data formed a distinct cluster, whereas the 12 and 24 hours groups were positioned closer to each other, indicating biochemical similarity in protein signal values. This result aligns with the protein data trends shown in Table 4 and the cluster bar plot, further confirming that protein part is the major factor influenced by variations in photoperiod.

The result can be explained biologically by increased activity in pathways linked to photosynthesis, including the Calvin cycle, nitrogen metabolism, and Photosystems I and II, when exposed to prolonged light. Zhang et al. (2024) claim that extended exposure to light activates pathways involved in protein biosynthesis, which is consistent with the spectral patterns found in this experiment.

Collectively, these results confirm that light exposure duration has an impact on the biochemical profile of Spirulina H53 strain, particularly in terms of protein content. This insight is crucial for optimizing cultivation conditions to enhance desired biochemical characteristics in Spirulina production, and may also be applied in the future to trace the origin and cultivation methods of Spirulina strains.

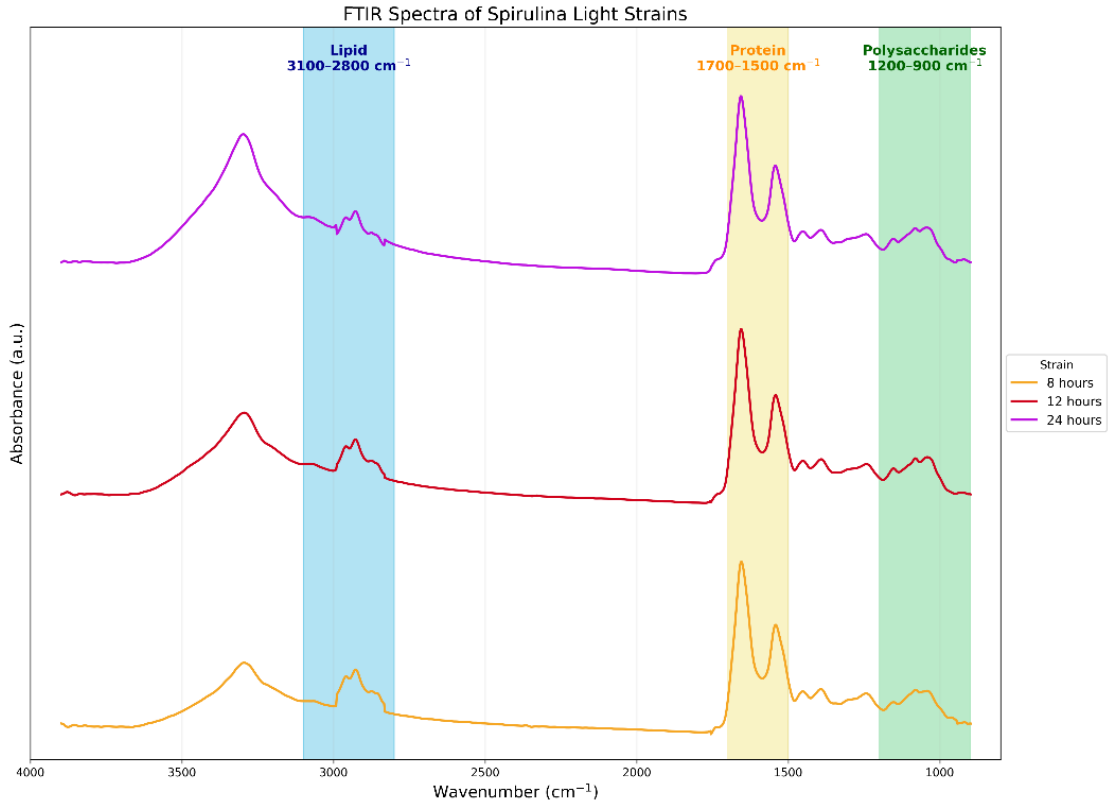

Figure 4.15 Average spectrum obtained from FTIR spectroscopy of Culture at 8, 12, and 24 hours under light conditions after smoothing, baseline correction, and extended multiplicative scatter correction (EMSC)

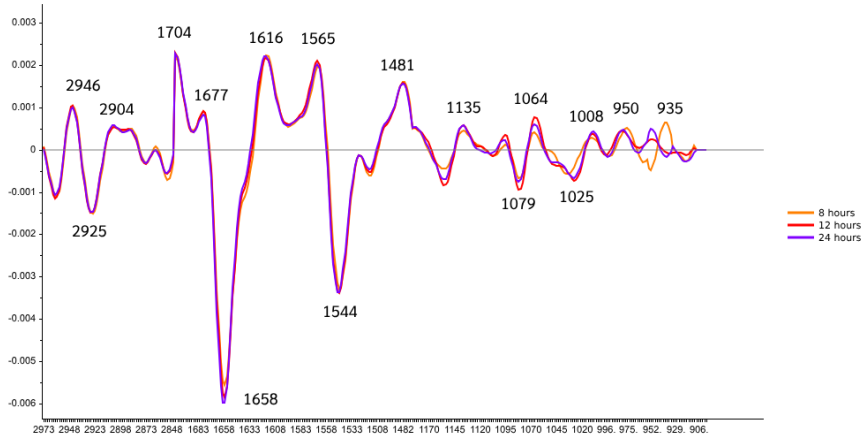

Figure 4.16 Second derivative of Photoperiod lengths treatment

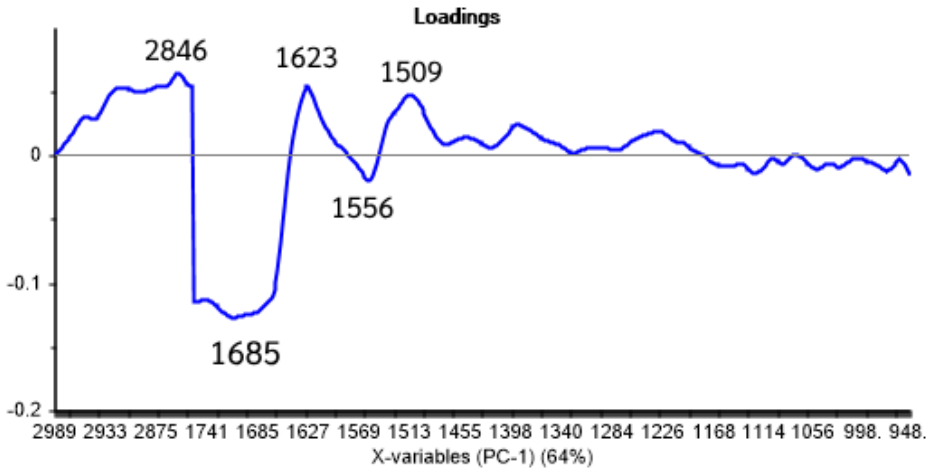

Figure 4.17 PCA loading plot (PC1) of FTIR spectra from photoperiod length treatments

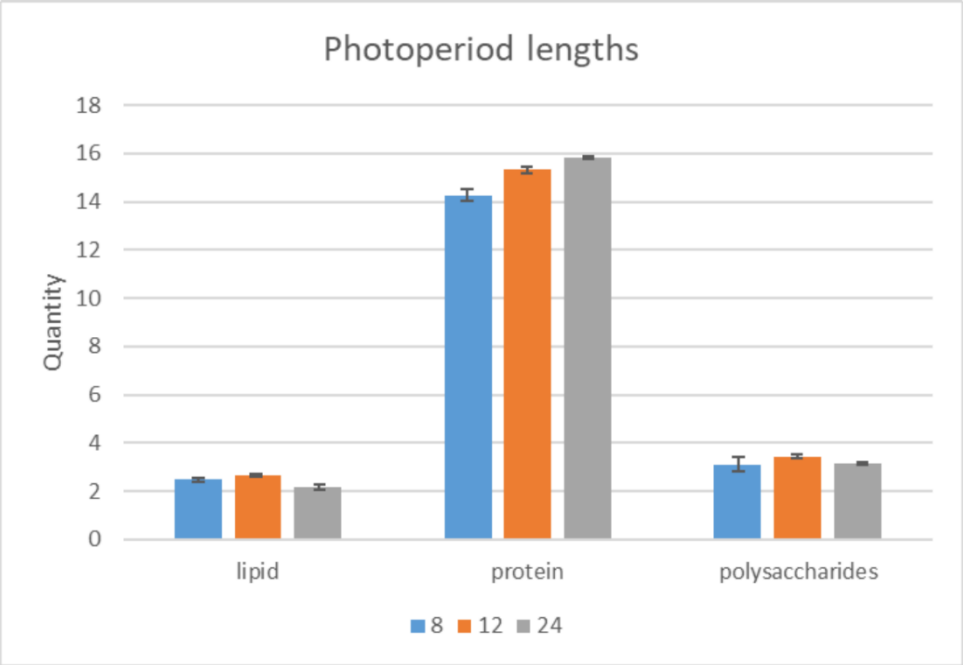

Figure 4.18 Biochemical composition under different photoperiod lengths

Table 4.1 The integral area of the average spectrum of Spirulina culture (H53 strain) from different photo periods

Biomolecule	photoperiod		
	8	12	24
C-H stretching of lipid	2.484 ± 0.08	2.666 ± 0.04	2.184 ± 0.10
C=O, N–H, C–N stretching of proteins	14.259 ± 0.26	15.350 ± 0.14	15.848 ± 0.04
C–O–C stretching of polysaccharides	3.099 ± 0.35	3.414 ± 0.08	3.16 ± 0.06

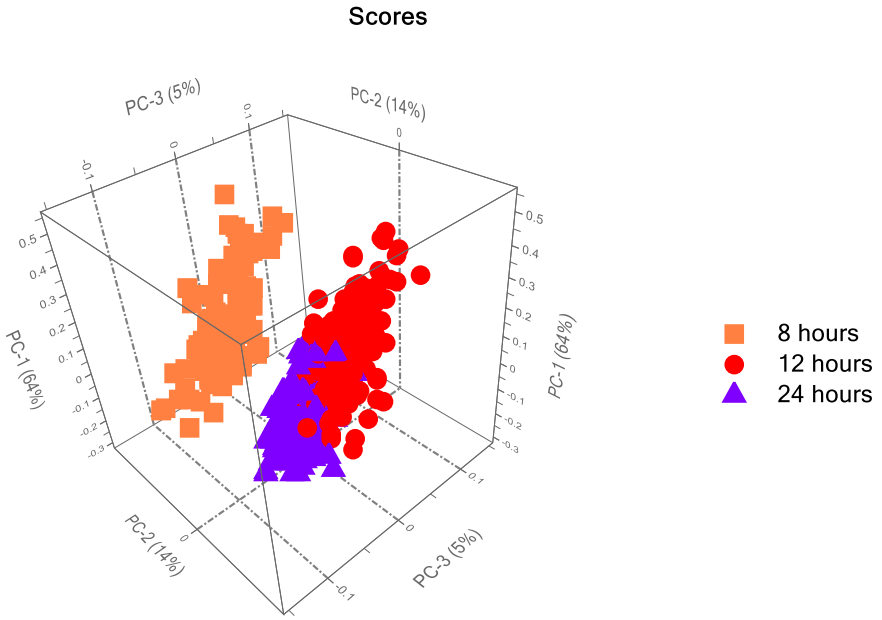

Figure 4.19 3D Model PCA of Spirulina Culture in Photoperiod lengths treatment

4.3 Effect of Water Types in Culture Medium on Biochemical Profile

Spirulina is well-known for the unique capacity to adapt to a wide range of conditions, including freshwater, brackish water, saltwater, and even soil (Ciferri, 1983). Spirulina H53 was cultivated indoors under controlled conditions using Zarrouk's medium with different water treatments, temperature (25°C), and pH 10 to investigate the influence of water source on biochemical composition. The variable in the culture medium consisted of two kinds of water: tap water and groundwater.

For both treatments, FTIR spectra in the 4000–400 cm^{-1} range were obtained (Figure 4.20). Visual inspection of the raw spectra showed an obvious difference in the carbohydrate region (1200–900 cm^{-1}), with higher intensity in the groundwater group. This implied a variation in the accumulation of polysaccharides. The protein region (1700–1500 cm^{-1}) and the carbohydrate region both showed stronger signal differences after applying second derivative transformation (Figure 4.21). These spectral regions

align with polysaccharide bands and amide bands, which are indicators of polysaccharides and proteins, respectively. The major peaks in various types of water were found in these two areas, as shown by the loading line plot (Figure 4.21). Polysaccharide-related signals near 1023 cm^{-1} were stronger in the groundwater group, whereas protein signals around 1648 cm^{-1} were greater in the tap water group.

These findings were supported by the cluster bar chart (Figure 4.23), which showed a noticeable increase in protein signal in the tap water condition, whereas the polysaccharide signal was markedly higher under the groundwater condition. Table 4 presents the quantitative absorbance values of major biomolecules: the protein region showed a higher average value in the tap water group (16.869 ± 0.06) compared to the groundwater group (13.885 ± 0.08), while the polysaccharide region showed the opposite trend, groundwater (10.272 ± 0.11) was significantly higher than tap water (4.805 ± 0.22). Lipid values were slightly higher in groundwater, but the variation was less pronounced (tap water: 2.349 ± 0.08; groundwater: 2.553 ± 0.04).

The cluster bar chart (Figure 4.23), which showed an obvious increase in the protein signal under tap water conditions while the polysaccharide signal was much greater under groundwater conditions, corroborated these findings. The quantitative absorbance values of the main biomolecules are shown in Table 4. The average value of the protein region was higher in the tap water group (16.869 ± 0.06) than in the groundwater group (13.885 ± 0.08), while the polysaccharide region displayed the opposite trend, with groundwater (10.272 ± 0.11) being significantly higher than tap water (4.805 ± 0.22). Although the difference was less noticeable, groundwater had slightly higher lipid values (tap water: 2.349 ± 0.08; groundwater: 2.553 ± 0.04).

In the cluster bar chart (Figure 4.23), the absorbance values of the major biomolecules are shown in Table 4. The value of the protein region of tap water (16.869 ± 0.06) was higher than the groundwater (13.885 ± 0.08), while the

polysaccharide region displayed the opposite trend, with groundwater (10.272 ± 0.11) being higher than tap water (4.805 ± 0.22). Groundwater had slightly higher lipid values. (groundwater: 2.553 ± 0.04; tap water: 2.349 ± 0.08)

The 3D PCA plot (Figure 4.24) shows a clear difference between the two water groups based on their spectral features, confirming that the type of water greatly influences the overall biochemical profile of Spirulina. The difference is mainly due to variations in protein and polysaccharide signals. The separation is mainly driven by differences in protein and polysaccharide signals.

The results imply that the different mineral compositions of tap and groundwater may be the cause of the biochemical variations. While tap water contains chlorine, fluoride, and leftovers from water treatment processes, groundwater typically has a wider variety of minerals, such as calcium, magnesium, bicarbonate, sulfate, chloride, and nitrate (Moreno-Merino et al., 2022). Groundwater's mineral content may cause osmotic or ionic stress, which would cause Spirulina to adapt its metabolism due to osmoregulation. Spirulina has been reported to accumulate carbohydrates, especially polysaccharides, under such stress (Kebede, 1997; Rosales et al., 2005).

As a result, the unique spectral patterns found in this study represent the biochemical profile of Spirulina H53 strain in response to variations in water quality. Such insights not only contribute to the improvement of cultivation strategies for targeted biochemical outcomes but also offer potential for future traceability of cultivation conditions based on strain signatures.

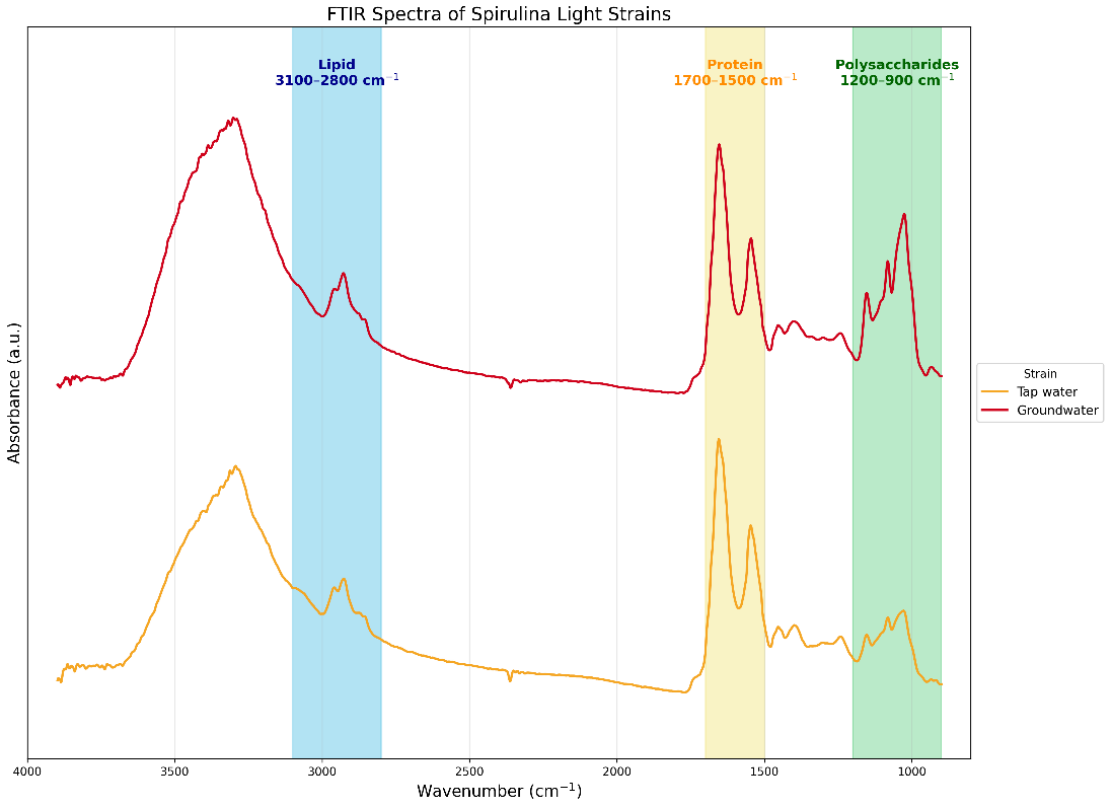

Figure 4.20 Average spectrum obtained from FTIR spectroscopy of Culture in Tap water and Groundwater after smoothing, baseline correction, and extended multiplicative scatter correction (EMSC)

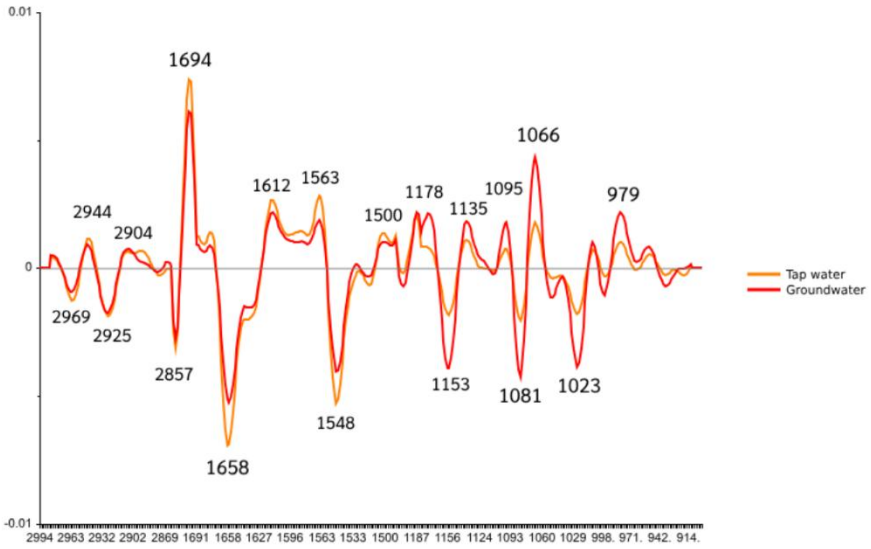

Figure 4.21 Second derivative of Photoperiod lengths treatment

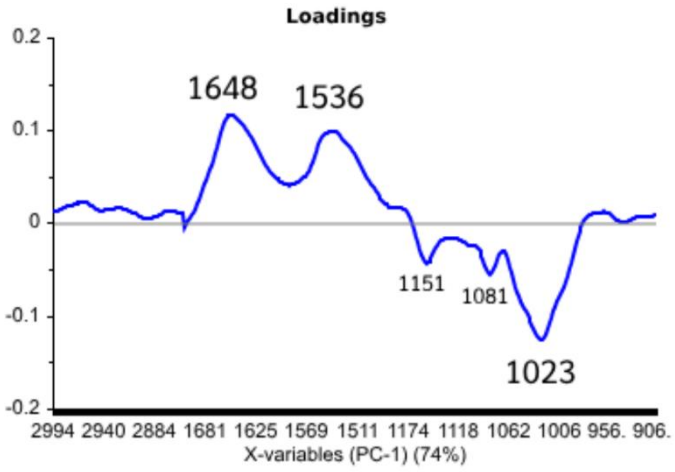

Figure 4.22 PCA loading plot (PC1) of FTIR spectra from Culture in Tap water and Ground water treatments

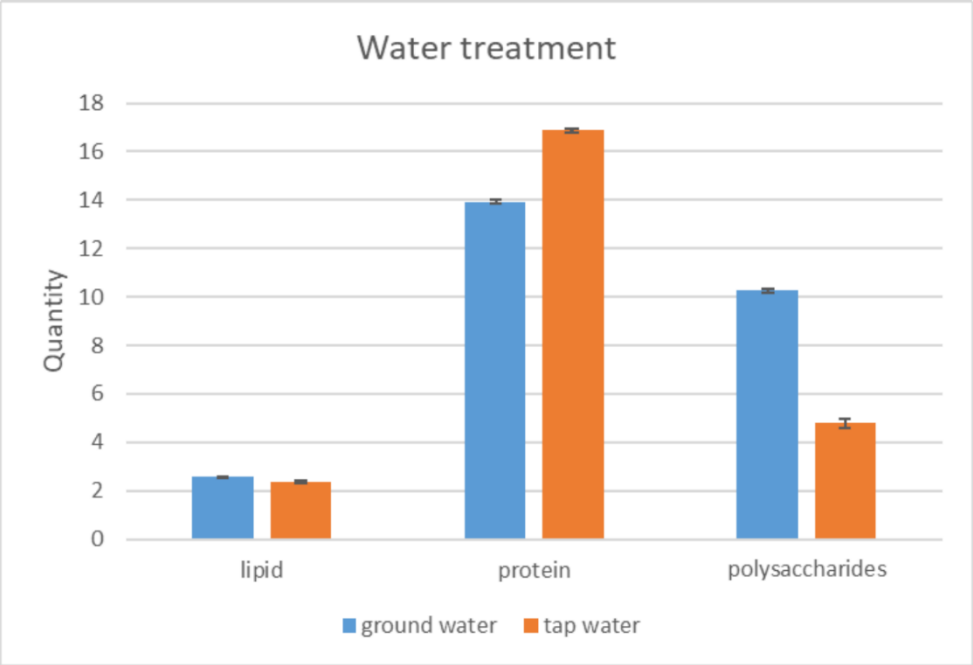

Figure 4.23 Biochemical composition under different water source treatment

Table 4.2 The integral area of average spectrum of Spirulina culture (H53 strain) from different water source treatment

Biomolecule	Water	
	Tap water	Ground water
C-H stretching of lipid	2.349 ± 0.08	2.553 ± 0.04
C=O, N–H, C–N stretching of proteins	16.869 ± 0.06	13.885 ± 0.08
C–O–C stretching of polysaccharides	4.805 ± 0.22	10.272 ± 0.11

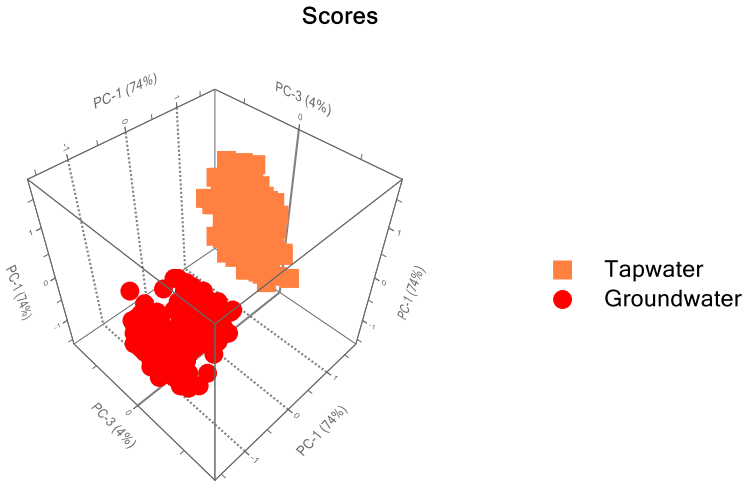

Figure 4.24 3D Model PCA of Spirulina Culture in water source treatment

4.4 Comparison of Indoor vs. Outdoor Cultivation Systems

The two main categories of Spirulina cultivation systems are indoor and outdoor, each with various environmental influences. In this study, 500 mL flasks were used to cultivate Spirulina H53 indoors under controlled conditions (Zarrouk's medium, temperature (25°C), and pH 10), while 100 L open systems were used in outdoor cultivation. The outdoor setting provided less control, like Zarrouk's medium, 100 L tank with air tube and Spirulina H53 strain. But the sunlight intensity, photoperiod, and temperatures are not controlled as in the indoor setting.

There were obvious differences between the two cultivation systems, especially in the polysaccharide region (1200–900 cm^{-1}), which appeared to be higher in the outdoor group, according to FTIR spectra obtained in the 4000–400 cm^{-1} range (Figure 4.25). According to previous results in water source comparisons, distinct differences were seen in the polysaccharide region (1200–900 cm^{-1}) and the protein region (1700–1500 cm^{-1}) following a process of second derivative transformation (Figure 4.26).

Two major peak zones for differentiating between indoor and outdoor cultivation were found by loading line analysis (Figure 4.27). These are the carbohydrate region, which is around 1022 cm^{-1} (polysaccharides), and the amide I region, which is around 1656 cm^{-1} (proteins). Cluster bar plots also showed that the polysaccharide signal was higher in outdoor cultures, and the protein signal was stronger in indoor cultures.

Table 4 provided quantitative data to support these observations. While the polysaccharide content showed the opposite trend. And outdoor cultures showed a higher value (5.517 ± 0.12) than indoor (3.781 ± 0.04). The protein absorbance was higher in indoor cultures (15.953 ± 0.11) than in outdoor cultures (15.21 ± 0.21). There were only minor variations in lipid levels between the two conditions.

It was found that environmental factors involving cultivation systems have an influence on the biochemical profiles by the 3D PCA model (Figure 4.29), which separated the indoor and outdoor groups. This supports previous results that stress situations, including photo-inhibition, can result from changes in the environment in outdoor systems, including intense light exposure, photoperiod variation, and temperature shifts (Juneja et al., 2013; Soni et al., 2017; Richmond et al., 1986).

It's interesting to realize that this trend aligns with previous results sections. In the photoperiod length treatment, the protein signals were the major variable. Also, the water source treatment, both protein and polysaccharide regions, was affected. And in this cultivation treatment comparison. The biochemical profile in protein and polysaccharides regions has variation. This pattern suggests that these two regions are major biochemical profiles that vary for environmental effects on Spirulina H53 strain.

These results support that Spirulina's biochemical profile is influenced by factors in cultivation systems, whether they are natural or controlled. More strategic cultivation planning is made possible by an understanding of how various systems affect biochemical profiles. These results may also help with traceability of cultivation conditions or uniquify Spirulina strains hereafter by using FTIR spectral fingerprints.

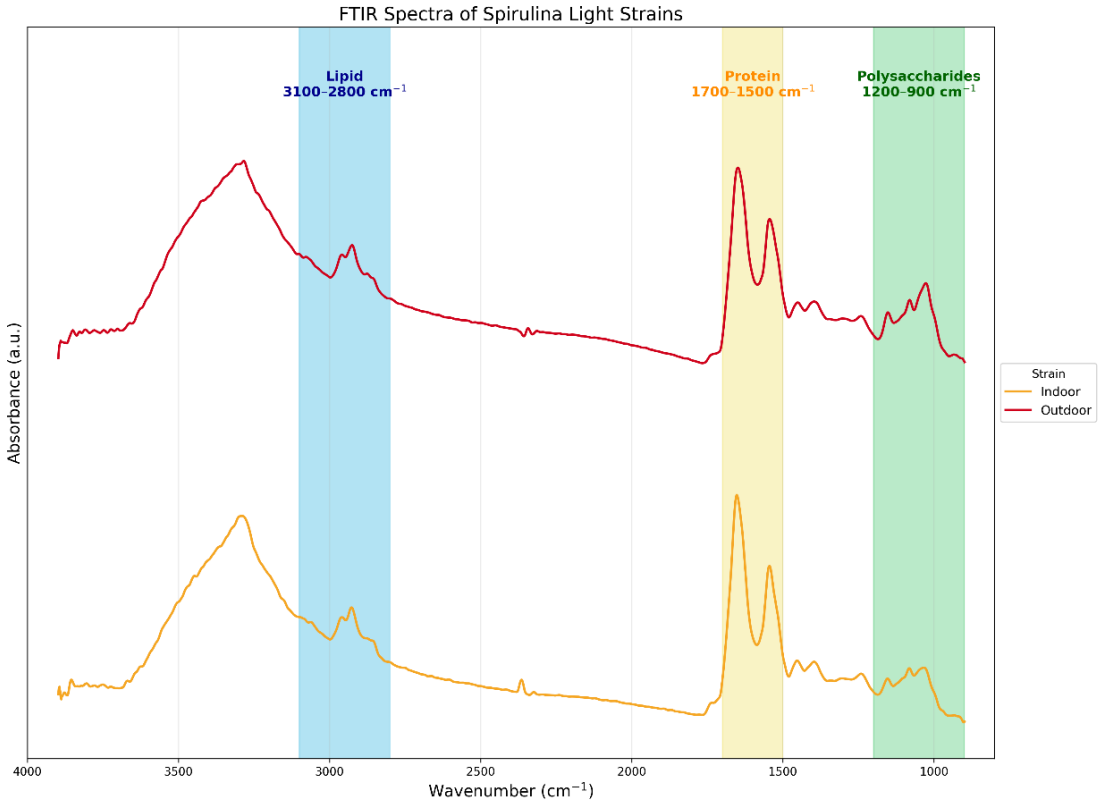

Figure 4.25 Average spectrum obtained from FTIR spectroscopy of Culture in indoor and outdoor conditions after smoothing, baseline correction, and extended multiplicative scatter correction (EMSC)

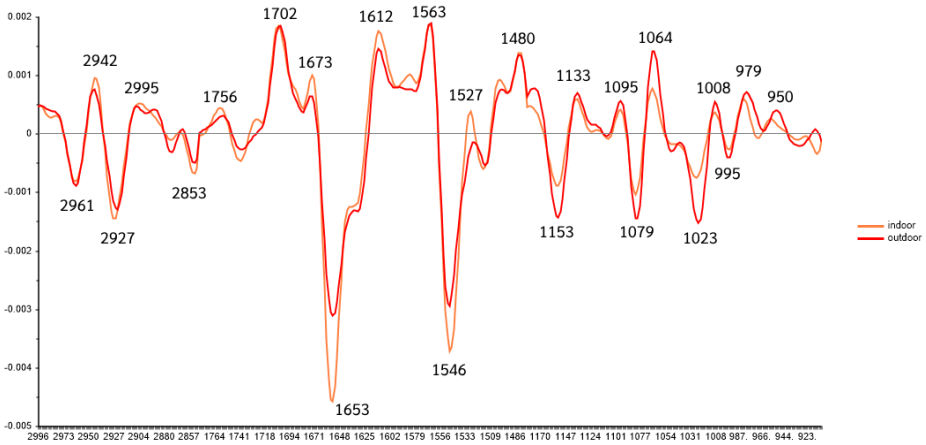

Figure 4.26 Second derivative of Culture in indoor and outdoor conditions

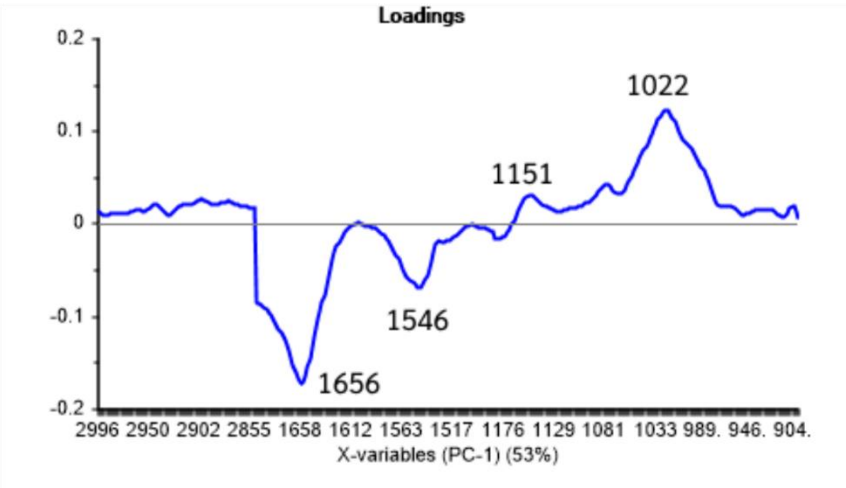

Figure 4.27 PCA loading plot (PC1) of FTIR spectra from Culture in indoor and outdoor conditions

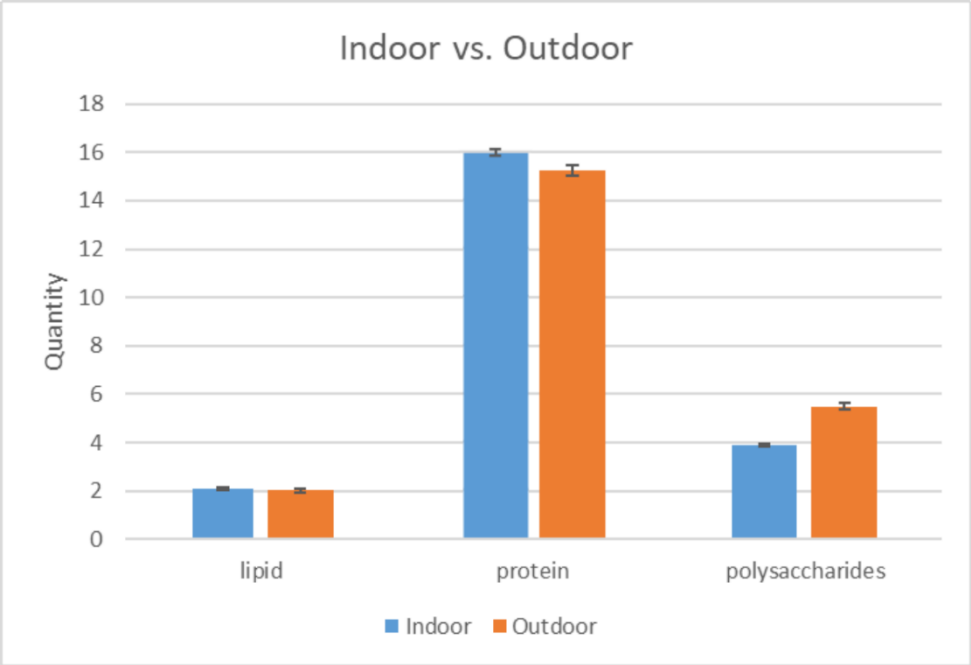

Figure 4.28 Biochemical composition under different Culture in indoor and outdoor conditions

Table 4.3 The integral area of average spectrum of Spirulina culture (H53 strain) from different indoor and outdoor conditions

Biomolecule	Culture	
	Indoor	Outdoor
C-H stretching of lipid	2.107 ± 0.05	2.039 ± 0.06
C=O, N–H, C–N stretching of proteins	15.953 ± 0.11	15.321 ± 0.21
C–O–C stretching of polysaccharides	3.781 ± 0.04	5.517 ± 0.12

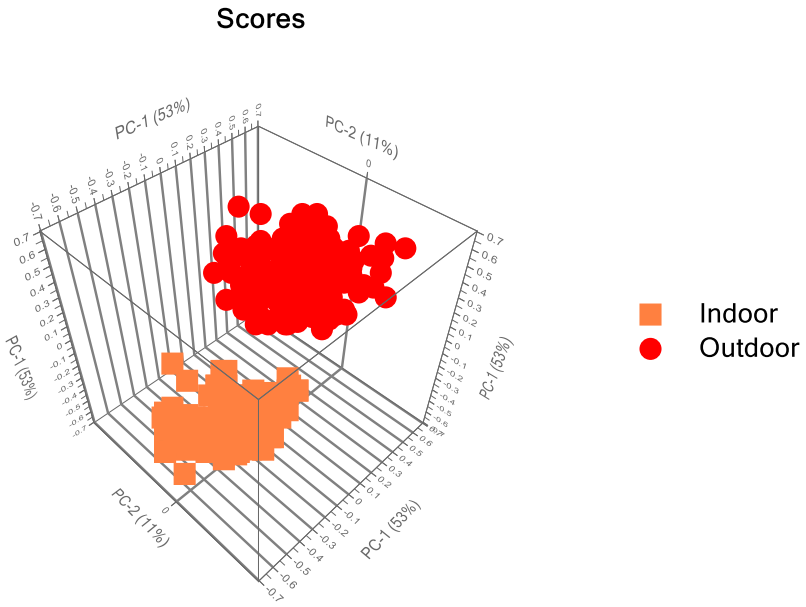

Figure 4.29 3D Model PCA of Spirulina Culture in Indoor and Outdoor cultured conditions